Viscous Transonic Airfoil Flow Simulation *)

Jose M. LONGO, Wolfgang SCHMIDT, Dornier, Friedrichshafen,
Antony JAMESON, Princeton University/USA**)

Summary: The present paper describes a method for the calculation of subsonic and transonic viscous flow over airfoils using the displacement surface concept. This modelling technique uses a fast multigrid solver for the full potential equation and laminar and turbulent boundary-layer integral methods. In addition, special models for transition, laminar or turbulent separation bubbles and trailing edge treatment have been selected. However, the flow is limited to small parts of trailing edge-type separation. The present paper deals with some theoretical features in a short description and shows computed results compared with experimental data and other methods.

Numerische Simulation reibungsbehafteter transsonischer Profilströmungen

Übersicht: Die vorliegende Arbeit beschreibt eine theoretische Methode zur Berechnung der reibungsbehafteten Profil-strömung im Unter- und Transschall. Die Simulation beruht auf der Lösung der kompressiblen Potentialgleichung, den kompressiblen Grenzschichtgleichungen und dem Verdrängungsdickenkonzept als Wechselwirkungsmodell. Die Potential-gleichung wird durch einen sehr schnellen Multi-Grid-Algorithmus gelöst, die laminaren und turbulenten Grenzschicht-gleichungen jeweils durch effiziente Integralmethoden. Zusätzlich werden spezielle Modelle zur Bestimmung von Transition, von laminaren oder turbulenten Ablöseblasen und zur Hinterkantenbehandlung eingesetzt. Die Anwendbarkeit der vor-liegenden Methode ist beschränkt auf stationäre Strömungen ohne oder mit mäßiger Hinterkanten-Ablösung. Neben einer Zusammenstellung der wesentlichen theoretischen Grundlagen wird eine Reihe von beispielhaften theoretischen Nach-rechnungen gezeigt und mit Windkanal-Meßergebnissen verglichen.

1. Introduction

In the past ten years transonic flow about airfoils has become a large range of interest. While transonic airfoil design is playing an important role in present day commercial airplane efficiency, the increase in transonic maneuver limits of fighter aircraft due to transonic wing design has been proven in flight for various prototypes. This transonic wing technology is nearly totally based on the availability of computational methods for design and analysis in transonic flow. Since present day wind tunnels are limited in *Reynolds* number, but viscous effects on transonic airfoils proved to be extremely important for performance, reliable computational methods for viscous transonic flow are of extremely high importance.

Basically, two approaches are possible to simulate these flows, either *Navier-Stokes* solutions or interacting flow modelling using an inviscid method and a boundary-layer theory. *Navier-Stokes* solutions are limited in engineering use presently due to rather high computational cost and partially lack of physical understanding, e.g. turbulence modelling. Although limited in the range of application, the interacting flow modelling using a full potential solver for the inviscid flow with some modelling of the trailing edge flow and shocks has been successfully applied by *Lock* [1], *Melnik* [2] and others. More recently, modelling techniques using the full *Euler* equations and inverse boundary-layer methods have been successfully developed and applied by *Whitflied, Jameson* and *Schmidt* [3].

The present approach consists of the iterative application of a transonic potential flow method and a boundary-layer part with semi-empirical models for separated regions using the displacement thickness concept [4]. The potential flow method is discussed first, followed by a description of the integral boundary-layer methods. The method used to couple the viscid-inviscid solutions is then described, followed by computed results for supercritical flows over airfoils for which experimental surface pressure and boundary-layer data are available.

2. Nomenclature

c	chord length
c_D	drag coefficient
C_E	entrainment coefficient
c_L	lift coefficient
c_f	skin friction coefficient $(= 2\,\tau_w/\varrho U_e^2)$
c_p	pressure coefficient
H	shape parameter $(= \delta^*/\Theta)$
H^*	shape parameter $(= \delta^*/\Theta^*)$
H_i	shape parameter

$$\left[= \frac{1}{\Theta} \int_0^\delta \frac{\varrho}{\varrho_c}\left(1 - \frac{U}{U_e}\right) dy \right]$$

H_i^*	shape parameter $(= \delta_i^*/\Theta^*)$
l_{sep}	separation length
M	*Mach* number
n	normal direction
Re	*Reynolds* number
s, ds	arc length
U	velocity
δ^*	displacement thickness

$$\left[= \int_0^\delta \left(1 - \frac{\varrho U}{\varrho_e U_e}\right) dy \right]$$

$$\delta_i{}^* \quad = \int_0^\delta \left(1 - \frac{U}{U_e}\right) dy$$

Θ^* momentum thickness

$$\left[= \int_0^\delta \frac{\varrho U}{\varrho_e U_e} \left(1 - \frac{U}{U_e}\right) dy \right]$$

ω relaxation factor
μ dynamic viscosity
Ω dissipation integral

$$\left\{ = \frac{1}{\varrho_e U_e} \int_0^\delta \mu \left[\frac{\partial (U/U_e)}{\partial y} \right]^2 dy \right\}$$

Φ potential
ϱ density

Subscripts

e value at edge of boundary layer
R reattachment
sep   separation
ts   transition
∞ free stream condition
α angle of attack

3. Potential Flow Method

The inviscid transonic potential flow is computed using *Jameson*'s multiple grid alternating direction technique [5]. The potential flow approximation has been found to give useful predictions in practice for transonic flow past an airfoil containing shock waves of moderate strength. The potential flow equation is treated in the conservation form:

$$(1) \quad \frac{\partial}{\partial x} (\varrho u) + \frac{\partial}{\partial y} (\varrho v) = 0,$$

where $u = \Phi_x$; $v = \Phi_y$.

At the profile, the potential satifies the *Neumann* boundary condition:

$$(2) \quad \partial \Phi / \partial n = 0.$$

The discrete approximation used is a rotated central difference scheme with an artificial viscosity which introduces an upwind bias throughout the supersonic zone. Time-dependent terms have been added to embed the steady-state equation in a convergent time-dependent process. The solution of the resulting set of nonlinear difference equations is done by the multiple grid method. This technique uses a fine grid to evaluate the residuals while the corrections are calculated in a coarse grid. The main advantage of this technique is that it treats the errors in the proper band i.e. high frequency errors are smoothened in the fine grid while low frequency errors are smoothened in the coarse grids. The difficulties that appear in this kind of method due to insufficient smoothing of the error in the fine grids before passing to coarser grids have been avoided using an alternating direction method as

solution with its smoothing properties. The method can treat arbitrarily shaped airfoil sections by means of conformal mapping of the exterior of the airfoil onto the interior of a unit circle. FIG. 1 shows the resulting mesh (Type 0) for the case of the NACA 0012 airfoil.

4. Viscous Flow Simulations

Viscous flow is simulated by coupling the inviscid code to a set of boundary-layer methods. The different boundary-layer methods as well as the iteration scheme are based on the work of *S. Leicher* [6]. In the present paper we will only sketch the basic ideas.

4.1. Laminar Boundary-Layer Method

A two dimensional version of *Stock*'s compressible laminar boundary-layer method [7] is used. This integral method uses for the evaluation of the integral thickness one parameter velocity profiles based on the similar solutions of the boundary-layer equations. Compressibility effects are taking into account by means of the *Stewartson* transformation.

From the momentum equation and the moment of momentum equation we finally get the following system of equations:

$$(3) \quad \frac{d\Theta}{ds} = \frac{c_f}{2} - \frac{\Theta}{U_e} \frac{dU_e}{ds} (2 - M_e^2 + H),$$

$$\frac{da}{ds} = \frac{1}{\Theta_a{}^*} \left[2\Omega - \Theta_\Theta{}^* \frac{c_f}{2} \frac{1}{U_e} \frac{dU_e}{ds} \times \right.$$

$$\left. \times \{\Theta^*[3 - M_e^2 + 2(H^* - H_i{}^*)] - \Theta_\Theta{}^* \Theta (2 - M_e^2 + H)\} \right]$$

with

$$\Theta_a{}^* = \frac{d\Theta^*}{da} , \quad \Theta_\Theta{}^* = \frac{d\Theta^*}{d\Theta} ,$$

where a is the single parameter describing the velocity profiles.
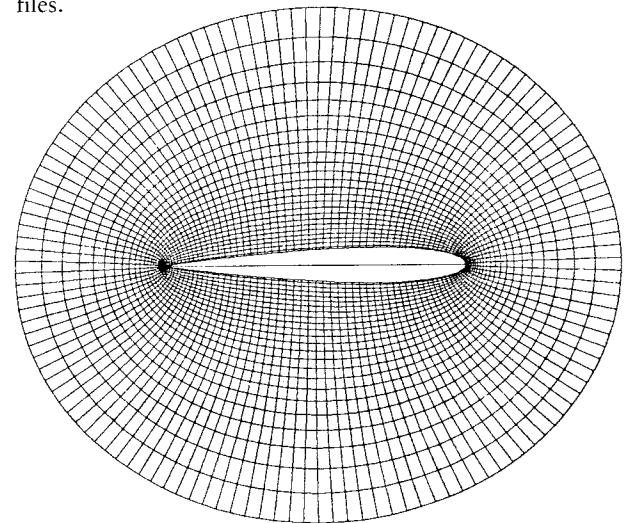

FIG. 1: 0 mesh, applied to the NACA 0012 airfoil

4.2. Transition, Laminar Separation and Reattachment Criteria

The transition from laminar to turbulent boundary layer is a very complex phenomenon depending on several parameters. However, in the present method we only take care of pressure gradient, local *Mach* number and *Reynolds* number. *Michel's* empirical correlation [8] modified by *Smith-Gamberoni* and *Cebeci-Smith* is used:

$$(4) \quad \begin{aligned} Re_{\Theta,ts} &= 1.174\, Re_{s,ts}^{0.46}, \\ 2\cdot 10^5 &< Re_{s,ts} < 2\cdot 10^7. \end{aligned}$$

Alternatively, transition can be specified by input. Laminar separation is assumed if $c_f = 0$ during the laminar boundary-layer computation. The criteria of *Goradia* and *Lyman* [9] is then used to determine if either laminar stall or short bubble type separation is apparent:

$$(5) \quad -0.002\, Re_{\Theta} - 1 < \frac{dM_e}{ds/c}.$$

For short and long bubbles *Horton's* [10] correlation is used for the separation bubble length l_{sep}:

$$(6) \quad l_{sep} = \frac{5\cdot 10^4 \cdot \Theta_{sep}}{Re_{\Theta sep}}.$$

Inside the bubble $U_e^3\,\Theta$ is assumed to ber constant leading to the reattachment momentum thickness

$$(7) \quad \Theta_R = \Theta_{sep}\frac{U_{e\,sep}^3}{U_{e\,R}^3}.$$

No model is available if bubble burst is indicated. After reattachment the computation starts with the calculations of the turbulent boundary layer setting the shape parameter H to a value of 1.55.

4.3. Turbulent Boundary Layer

The turbulent boundary-layer method used for attached flow is essentially the lag-entrainment integral method of *Horton* [11], with suitable modifications for compressibility. It consists of the simultaneous integration of the momentum integral and entrainment equations together with a third empirical differential equation which takes into account the effect upon the entrainment rate of the upstream history of the turbulence:

Momentum:

$$(8) \quad \frac{d}{ds}(\varrho_e U_e^2 \Theta) = \varrho_e U_e^2\left[c_f/2 - \frac{\delta^*}{U_e}\frac{dU_e}{ds}\right].$$

Entrainment:

$$(9) \quad \frac{d}{ds}\left[\varrho_e U_e(\delta - \delta^*)\right] = \varrho_e U_e C_E,$$

$$(10) \quad \frac{dC_E}{ds} = \frac{0.014}{\Theta}\left[C_{Eeq} - C_E\right].$$

The empirical shape parameter and entrainment relations used are based on those of *Horton* [11] and are:

$$(11) \quad H_i = 0.88 + \left(\frac{0.591}{H_1 - 3.607}\right)^{0.4} \text{ for } H_1 \geqq 1.68$$

and

$$H_i = 0.88 + \left(\frac{0.92326}{H_1 - 3.244}\right)^{1/1.85} \text{ for } H_1 < 1.68,$$

where $H_1 = (\delta - \delta^*)/\Theta$ is *Head's* shape parameter. (This correspond to *Horton's* relations for $Re_\Theta = 10^4$.)

$$(12) \quad C_{Eeq} = \frac{0.057}{H_1 - 3.0}(c_f/c_{fi}).$$

In order to prevent the failure of the code due to the inability of standard boundary-layer methods to compute boundary-layer parameters beyond separation a constant value of the entrainment coefficient C_{Eeq} that corresponds to a shape parameter $H_{isep} = 4$ is used. The length scale Θ in Eq. (10) is set equal to the value of Θ at separation since this is a characteristic of the separated shear layer thickness. The momentum equation is discarded, and Θ and δ^* are calculated from the computed values of $(\delta - \delta^*)$. Skin friction c_f is calculated from a compressible form of the *Ludwieg-Tillmann* relation

$$(13) \quad c_f = \frac{0.246}{(1 + 0.13\,M_e^2)Re^{0.268}\,10^{-0.678H_i}} = (c_f/c_{fi})\,c_{fi},$$

where

$$Re_\Theta = \frac{\varrho_e U_e \Theta}{\mu_e}, \quad c_f/c_{fi} = (1 + 0.130\,M_e^2)^{-1}.$$

While "re-attachment" is simulated by evaluating dH_i/ds at each step in the separated flow from the shape parameter equation, and allowing H_i to become less than H_{isep} once the derivative becomes negative.

But in general, the application of the numerical method is limited to flows where the turbulent boundary layer is attached over the airfoil surface except for small portions.

5. Iterative Simulation Procedure

The present code has a high flexibility in its topographical structure. The main program controls the general input, output, plots, and iteration. In addition there are two secondary control programs which direct the potential flow and boundary-layer models, respectively. Each of both secondary control programs contains special input and output routines, so that they can be easily combined with any other potential or viscous solver. A cyclic iterative procedure between the potential flow method and the boundary-layer part is used to finally provide the converged viscous solu-

tion. Both regions are computed separately but sequentially until both are converged to solutions with common boundary values. The following sequence is used:

— after one to three MAD cycles in the inviscid potential solver for the equivalent airfoil shape,

— the displacement thickness distribution is computed for the given pressure distribution by means of the viscous method described in the preceding pages,

— the relaxed displacement thickness

$$(14) \quad \delta^* = \omega\delta^*_{\text{new}} + (1 - \omega)\delta^*_{\text{old}}$$

is either added to the physical shape and for this shape the inviscid flow field is computed, again, using only one to three MAD cycles,

— then, new viscous quantities are computed and the whole cycle between viscous and inviscid computations is continued until either the convergence criterion is reached or the cycle is stopped by the user. The convergence criterion is based on the relative difference between the lift coefficient in two consecutive cycles plus a bound for the residual in the MAD method.

Alternatively, smoothing of the displacement thickness can be applied before the relaxation procedure.

It was well exposed by *Lock* [1] that in this kind of methods some empirical feature have to be introduced to deal with the trailing edge region. In the present method it has been assumed that c_f is equal zero just at the trailing edge, thus the pressure distributions of the aft part of the airfoil are forced to satisfy this condition.

6. Force and Moment Computation

Lift and moment coefficients are computed by integrating the surface pressure and skin friction. Drag is computed using the approach of *Squire* and *Young* [12] for compressible flow and adding the losses through the shock, that is:

$$c_D = c_{\text{DSY}} + c_{\text{DW}}.$$

In addition, drag is computed by integration of surface pressure and skin friction. For subcritical cases it was found that both methods gave the same answer, while in supercritical flows the integration of skin friction and pressure seems to underpredict the drag, compared with the above equation and also with measurements. In the present method, no computation through the wake is needed due to the special trailing edge treatment.

7. Examples

In general, the results presented here have been obtained using 160×32 mesh points. For the inviscid solution we used the fully conservative second order accurate scheme [5]. The solutions were obtained with a residual of 10^{-5} in the inviscid part and a convergence criterion of $\Delta c_L \approx 0.1\%$ for the interacting cycle. Typical CPU times for these cases on an IBM-3031 computer are between 2 and 5 minutes.

CAST 7 (DO-A1)

CAST 7 is a 12% thick transonic airfoil, designed by Dornier, which has been tested in several European wind tunnels according to the experimental program suggested by Garteur. Experimental results are presented here from the ONERA-S3MA tunnel [13], covering a traverse in incidence at three *Mach* numbers (i.e. 0.60; 0.70 and 0.76), giving
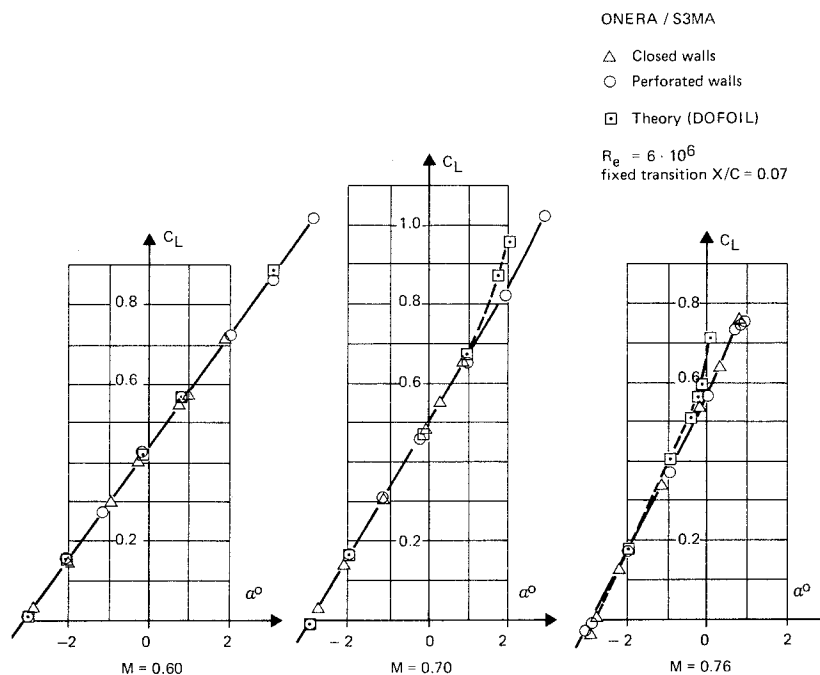

FIG. 2: CAST 7 (DO-A1), lift versus α comparison

values of c_L from 0.0 to 0.8. The main part of the study is concerned with the results with fixed transition at 0.07 on both surfaces. Additional points were obtained with free transition. *Reynolds* number for all cases was 6.0×10^6.

The variation of lift coefficient (c_L) with the angle of incidence (α) for the three *Mach* numbers is shown in FIG. 2.

We see that the values of c_L for low subsonic flow are in excellent agreement with the experiment up to the limit of the potential flow theory. For high subsonic flow $(M_\infty = 0.76)$ there is a slight overprediction of the c_L versus α slope for lower c_L values. Discrepancies become greater for c_L above dragrise. This is well understandable taking in mind that the pressure rise for an isentropic shock is always greather than that for a true (*Rankine-Hugoniot*) shock, by an amount which becomes appreciable when the upstream *Mach* number M_1 exceeds about 1.2, a value well below that at which shock-induced boundary-layer separation would be expected $(M_1 = 1.3$ to $1.4)$.

The variation of c_D with c_l, again, for the three free stream *Mach* numbers is shown in FIG. 3.

It is interesting to note that the trends of all the theoretical curves agree very well with the experimental ones until $c_L \approx 0.75$ while it is necessary to apply a shifting of 12 counts in order to match the same value of total drag for the three *Mach* numbers. This shifting is not completely understood with respect to other experiences with other airfoils (like RAE 2822 and NACA 0012) where for subcritical cases there was no difference or never more than one count between experiment and theory.

In FIG. 4 we show the variation of pitching moment with c_L for the three *Mach* numbers. While the trends of the theoretical curves are again in quite good agreement whith the experimental ones, the general level of c_m is overestimated.
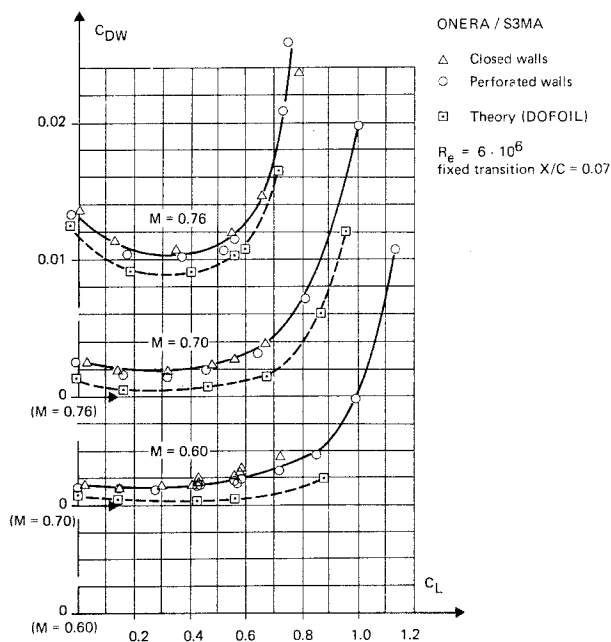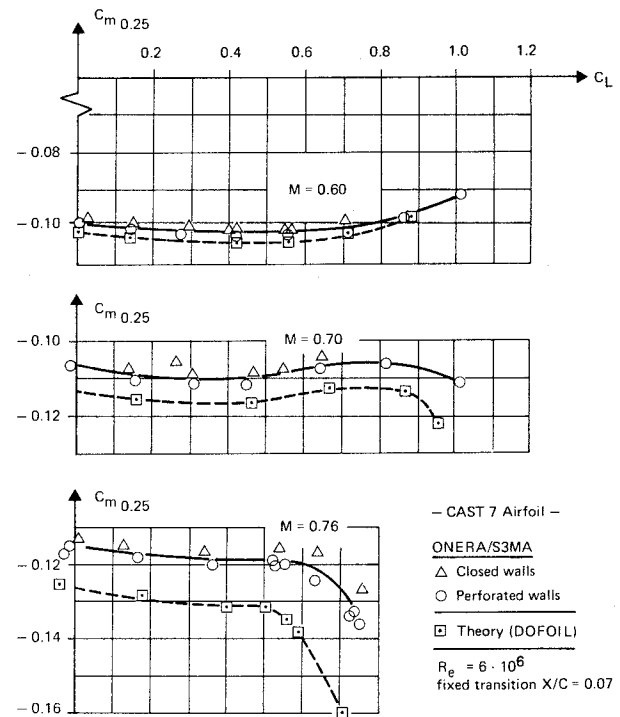
FIG. 3: CAST 7 (DO-A1), lift versus drag comparison

FIG. 4: CAST 7 (DO-A1), lift versus moment comparison

These differences, which increase with the free stream *Mach* number are not so easy to explain but may be due to small differences in the surface pressure of the rear part of the airfoil, which occur when lift is matched for high subsonic flow.

A comparison between theoretical and experimental pressure distribution is shown in FIG. 5.

Remembering that the present case was computed under the same condition as in the experiment, i.e. without any *Mach* number or/and incidence correction, the double shock flow pattern has been captured quite well. The shock positions are something backward which is correlated with the differences in total lift. Excellent agreement has been found for the entire upper surface and for the trailing edge pressure itself. As we mentioned already above, the program slightly overpredicts the pressure on the lower surface aft portion.

In FIG. 6 the solution from the VGK code [14] has been compared with the present approach and with the experimental data. Comparison has been carried out for the same lift coefficient. Agreement between both theories is quite good, also concerning incidence correction (there is a difference of only 0.05 degree). While the present code underpredicts the rear loading, the VGK underpredicts the lower surface pressure just below the maximum lower surface peak. Regarding the differences with the experimental pressure we conclude the following explanation: (1) The discrepancies of the front part upper surface are due to the transition band. (2) The missing of the double shock system seems to come from the potential flow theory applied. (3) The differences on the lower surface front part are necessary to compensate for the double shock in order to get the same c_L as in the experiment.
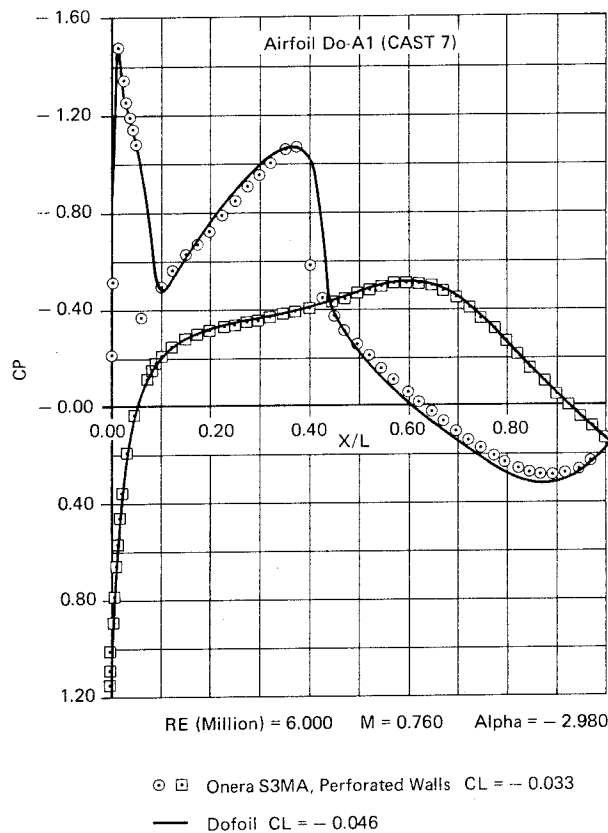
RE (Million) = 6.000   M = 0.760   Alpha = − 2.980

⊙ ⊡   Onera S3MA, Perforated Walls   CL = − 0.033

———   Dofoil CL = − 0.046
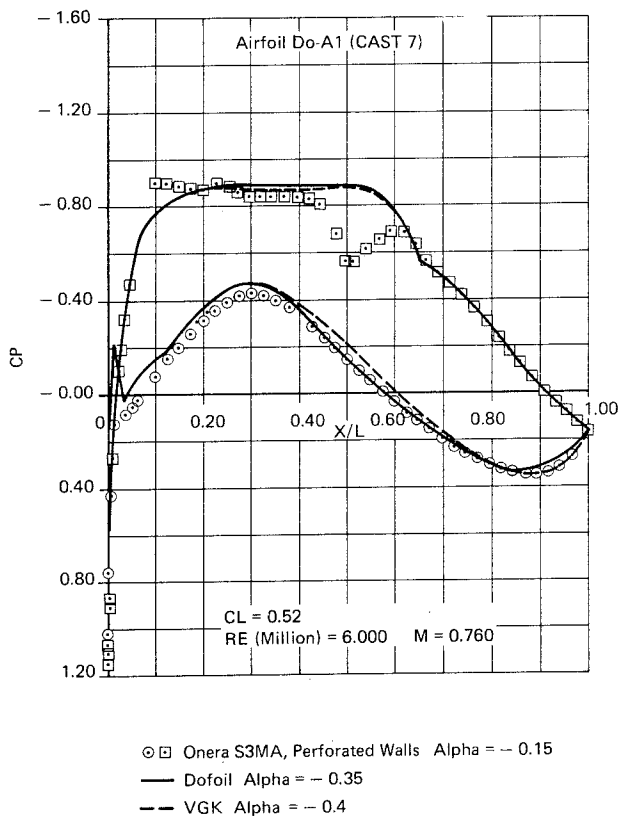
FIG. 5:   Pressure distribution comparison

FIG. 7 shows a comparison between three different theories and experimental results in total forces prediction. For this purpose, one of the most widely used codes, the BGKJ [15], with a very simple viscous effect formulation, and on the other hand the VGK code [16] which can be considered as a strong-interaction viscous effects code have been chosen. These results are reproduced from [14]. The present approach has from the point of view of its viscous effects formulation an intermediate option, more close to the BGKJ than the last one. However, regarding the results, the

CAST 7 / M_∞ = 0.76
RE : 6 10^6 T.S.: 0.07 X/C

Onera/S3MA   ⊙
BGKJ (NC)   —·—
VGK   — — —
Dofoil   ———

CL = 0.52
RE (Million) = 6.000   M = 0.760

⊙ ⊡ Onera S3MA, Perforated Walls Alpha = − 0.15
——— Dofoil Alpha = − 0.35
– – VGK Alpha = − 0.4

FIG. 6:   CAST 7 (DO-A1),
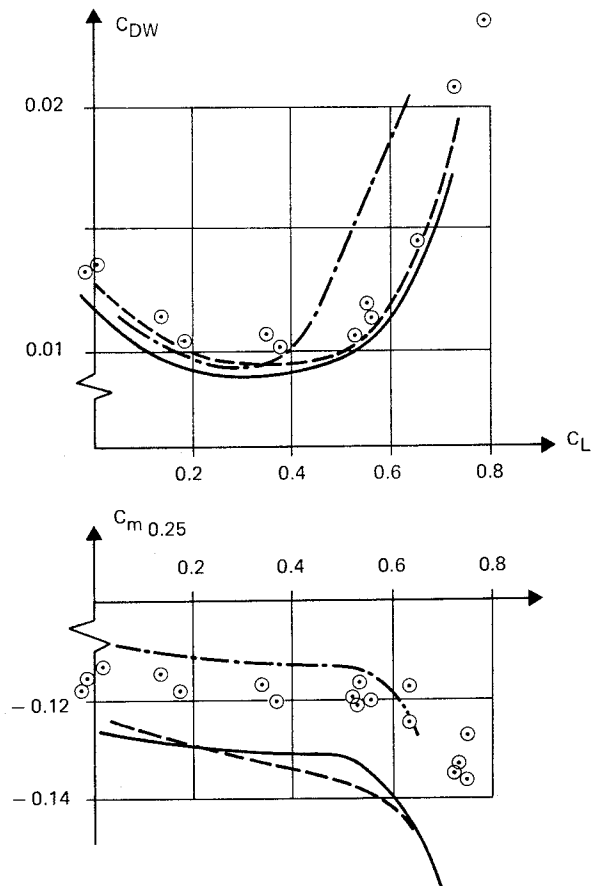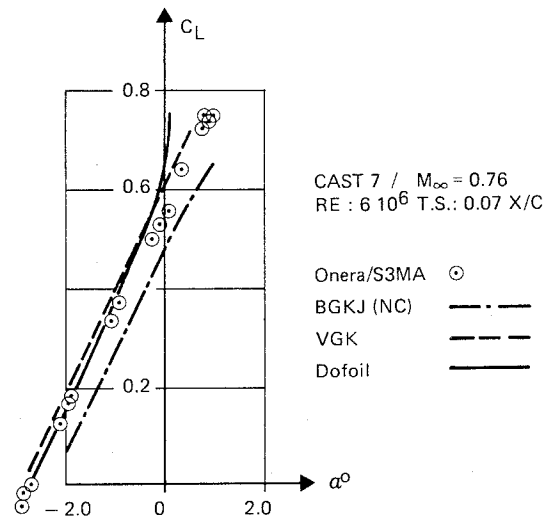pressure distribution comparison (α = − 0.15)

FIG. 7:   Total forces and moments comparison between
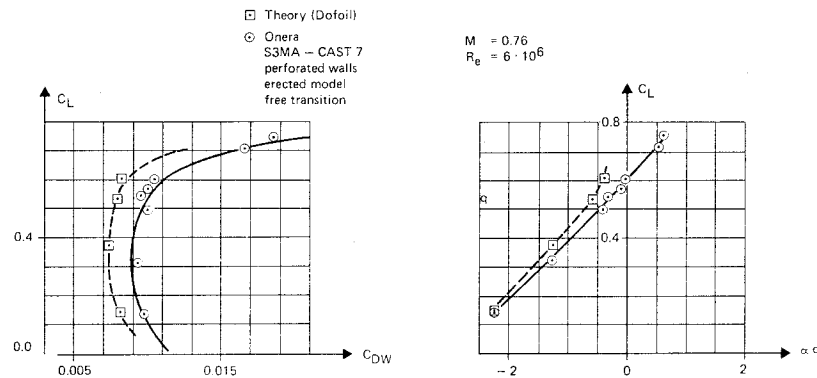different computer programs

FIG. 8: CAST 7 (DO-A1), total forces comparison (free transition)

Dofoil code provides practically the same accuracy as the VGK one using a much simpler and faster formulation. The variation of c_L with α is slightly overpredicted by both methods. Above $c_L = 0.6$ the partially conservative scheme (P–C) shows its advantages with respect to the fully conservative one used in the present formulation. However, this is only balancing the imperfectness of the full potential formulation. In the case of the BGKJ there is no agreement neither in level nor in shape with respect to the experiment. The pitching moment seems to be in magnitude extremely sensitive to the small differences in pressure found between theory and experiment. For this reason, all programs gave nearly the same accuracy. However, the BGKJ reproduces quite well the trend of the curve c_m versus c_L and has the smallest difference in level of all. The Dofoil code reproduces quite good the slope of the curve but the level of the c_m is off, while the VGK code is completely off as well in trends as in level. Finally, concerning the variation of c_D with c_L both programs, VGK and Dofoil, predict quite well the position of the drag-rise. Nevertheless, the level of drag provided by Dofoil is below the experimental answer and also below the VGK code. The trend of the curve of the present approach agrees better with the experiment than the VGK program. The BGKJ code overpredicts too much the drag-rise location.

As one exercise the capability of the present code to describe effects from transition position has been investigated. FIG. 8 shows the comparison between experiment and theory under free transition conditions.

We can see that the present approach overestimates the effects of the free transition. In fact, the differences between theory and experiment become greather as in the fixed transition cases. However from the qualitative point of view the results look reasonable: Moreover from the comparison of the two theoretical pressures with and without transition in FIG. 9 it can be concluded that the differences in pressure shape are in agreement with the physical phenomenon as for example the shock – laminar boundary-layer interaction. Unfortunally there is no information about natural transition location in the wind tunnel test in order to compare with the present results. The formulation adopted in the present approach to describe the natural transition seems to be highly influenced by the pressure gradient and for this reason the backward natural transition location is found and also due to this artificial increase of the laminar flow the estimation of the total forces becomes less accurate.

RAE 2822

The airfoil is a 12 % thick supercritical airfoil with a moderate amount of rear-loading. It was tested in the RAE 8×6 ft transonic tunnel [17] in which measurements of both, surface pressures and boundary-layer development, were carried out. The examples considered here were carried out at 6.5×10^6 *Reynolds* number and at nominal *Mach* numbers of 0.725 and 0.730. Transition was fixed in both cases at 0.03 chord.

The momentum displacement thickness, shape factor, and skin friction were determined from velocity-profile measurements, made at a number of locations on the model and the drag as well as in the previous examples was determined from wake rake measurements. All theoretical solutions were carried out at the measured lift coefficients. The
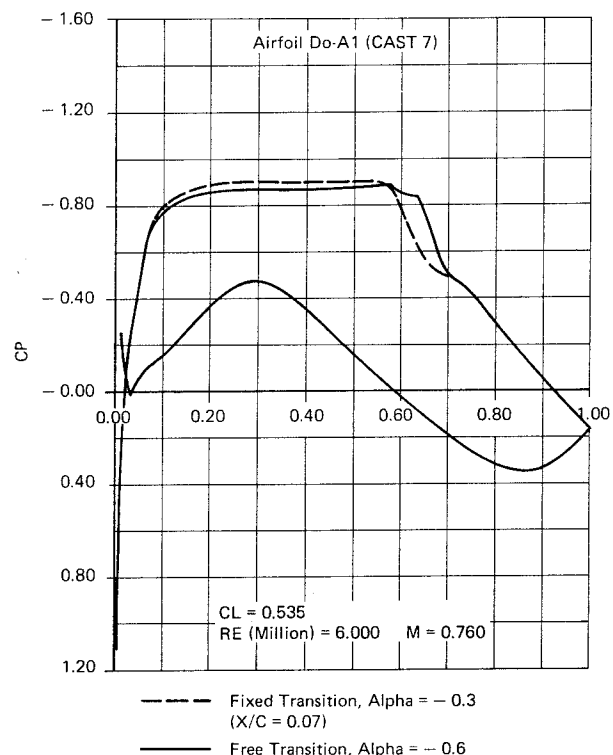

FIG. 9: Effect of the transition location on the pressure distribution
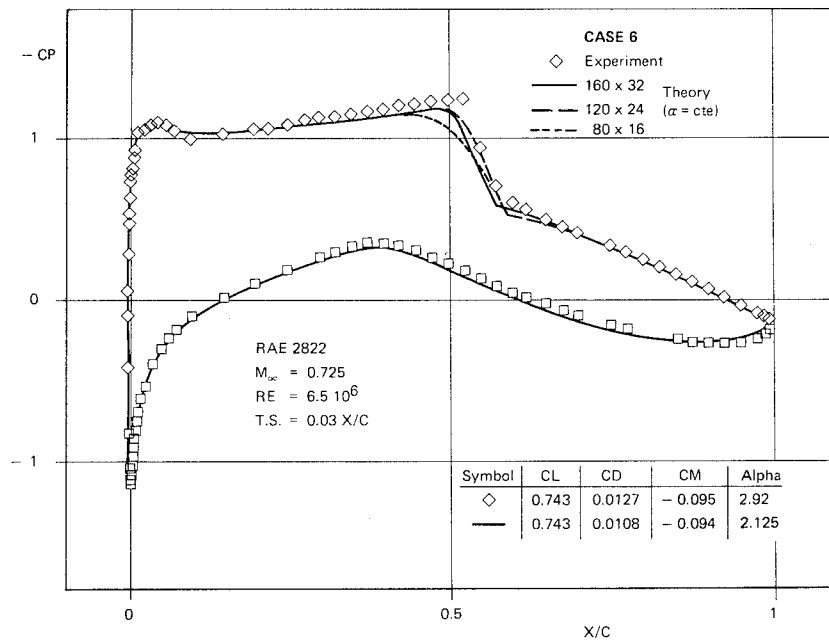
FIG. 10: RAE 2822, pressure distribution comparison (case 6)

pressure distribution for the $M_\infty = 0.725$ case is compared with experiment in FIG. 10.

The overall level of the pressure distributions on the airfoil is reasonably well predicted. The small discrepancies between theory and experiment over the forward part of the upper surface are probably due to both the transition roughness strip used and wall-interference effects. The underprediction of the pressure jump at the shock are due to wind-tunnel blockage as we will see later. In the same picture some indication of the influence on the number of points used in the potential solution on the final answer has been indicated. For this investigation the incidence was fixed at the value for which the standard mesh (160×32) provided the required c_L.

The boundary-layer development for this case is given in FIG. 11.

The overall agreement between theory and experiment is relatively good over the entire upper surface.
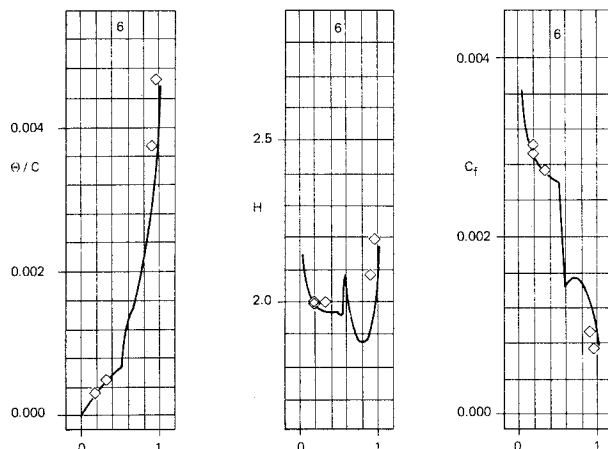
FIG. 12 shows the same case as before but now the theoretical answer has been obtained using a blockage correction in *Mach* number. At the same time this solution has been compared with the Grumfoil results [18] and with the viscid-
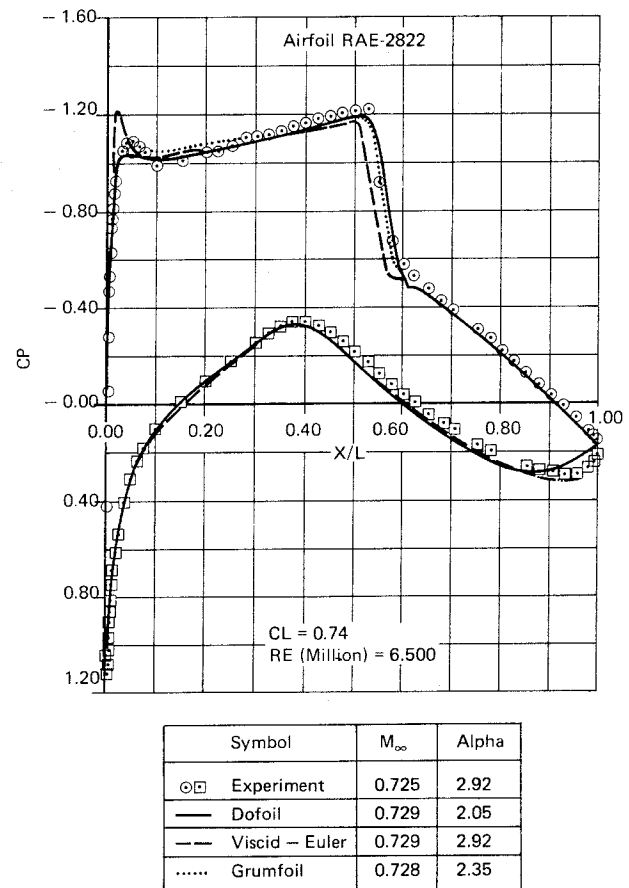

FIG. 11: RAE 2822, upper surface boundary layer parameters compared with experiment (case 6)

FIG. 12: RAE 2822, blockage corrections influence on pressure shape (case 6)

Euler ones [3]. In the case of the viscid-*Euler* and the present approach a blockage correction of $\Delta M = 0.004$ has been used following the recommendation of *R. Lock. Melnik*'s results correspond to a blockage correction of $\Delta M = 0.003$. It is important to note that both, the Grumfoil and the Dofoil solution have been carried out at the same experimental lift coefficient, while the viscid-*Euler* solution corresponds to the same incidence as the wind tunnel.

The overall agreement between Grumfoil and Dofoil results is quite good over the entire airfoil, with the only exception that Dofoil underestimates the rear loading in the aft part of the lower surface pressure of the airfoil.

The pressure distribution for the case tested at a *Mach* number of 0.73 is compared with the experiments and with the solution of *Le Balleur* [19] in FIG. 13. The picture also includes a first order scheme solution of the present approach. In all the three cases the overall level of the pressure distributions on the airfoil is reasonably well predicted. The discrepancies between theories and experiment on the front

of the upper surface can be justified in the same way as before. Concerning shock-wave location the best result is obtained by the first order Dofoil potential solution scheme, but at a smaller lift coefficient. The other two theoretical solutions overpredict the shock jump. In the case of *Le Balleur*'s results an overestimation of the c_p level behind the shock is produced. For the case of the present theory the overprediction of the shock jump is based on the aftward shock position. The boundary-layer development for this case is given in the same FIG. 13. The theoretical result corresponds to the solution with the standard version of the Dofoil code (i.e. 2nd order accurate scheme). The agreement between theory and experiment is again quite good. Shape factor and skin friction for this case are notoriously influenced by the overprediction of the shock pressure jump.

8. Conclusions

A new method was presented for the viscous transonic flow analysis. It seems to be a good engineering tool for the analy-

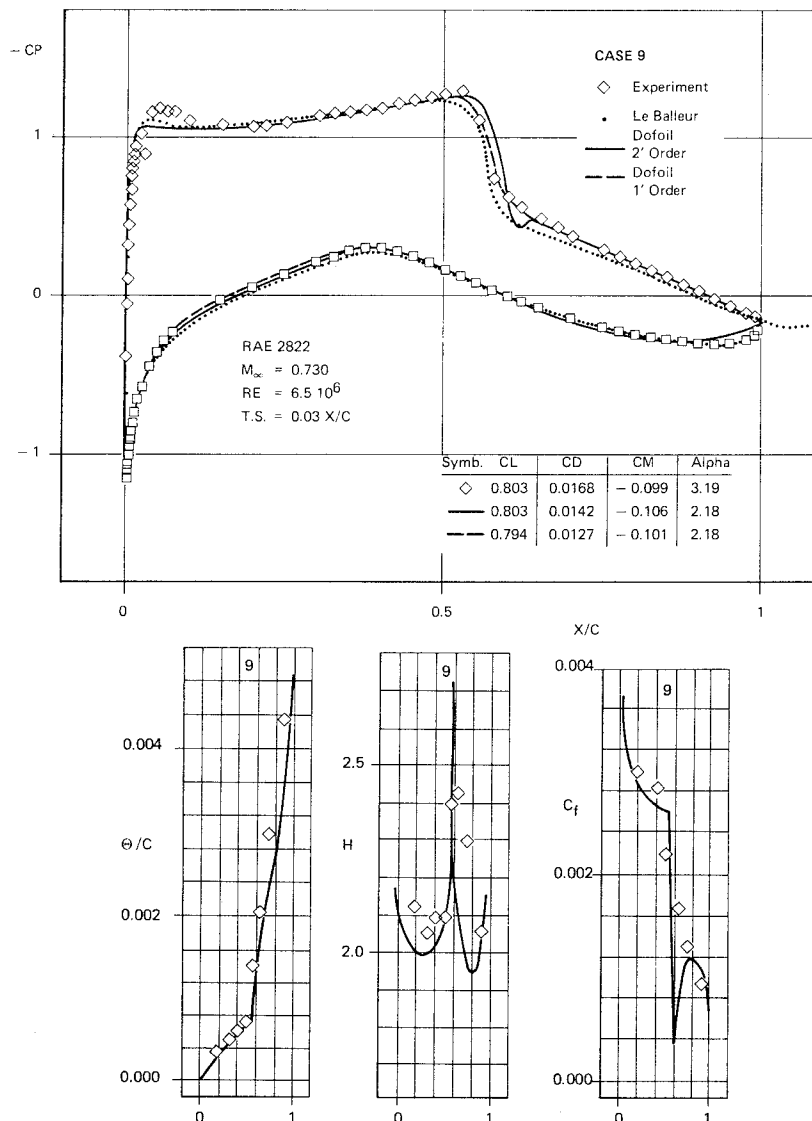| Symb.	CL	CD	CM	Alpha
◇	0.803	0.0168	− 0.099	3.19
——	0.803	0.0142	− 0.106	2.18
— —	0.794	0.0127	− 0.101	2.18

FIG. 13: RAE 2822, pressure distribution and boundary-layer comparison with experiment (case 9)

sis of airfoils in transonic flow due to its accuracy and fast resolution using a simple self-consistent formulation. Compared with the most widely known codes like Grumfoil, VGK or BGKJ, it seems to have the following advantages:

- a fast conservative inviscid full potential flow solver,
- a viscous model which includes the laminar boundary-layer part and transition as well as separation models,
- a fairly simple formulation to deal with the trailing edge which contemplate in an accurate way the effects of the wake.

Regarding its possible error sources we can say that mainly it contains the same as the other methods. From the point of view of the inviscid solver it uses the transonic potential flow formulation which deals with the transonic flow in an isentropic form. The fully conservative scheme produces an overprediction of the pressure jump at the foot of the shock and as well as the nonconservative formulation it has the problem of the nonunique solution (most of these problems can be solved by using the *Euler* method [1] and [3]).

From the point of view of the viscous part it does not include the proper formulation to deal with transonic turbulent flow separation, limiting the application of the code to no or small parts of trailing edge separation. While this is no basic restriction since large trailing edge separated regions are known to be unsteady and, thus, are outside of the scope of the present approach, the use of inverse boundary-layer methods instead of direct ones seems to give further improvement for this kind of problems [3].

References

[1] *R. L. Lock:* A review of methods for predicting viscous effects on aerfoils and wings at transonic speeds. AGARD Conf. Proc. 291 (1980), pp. 2.1 to 2.32.

[2] *R. E. Melnik:* Turbulent interactions on airfoils at transonic speeds – recent developments. AGARD Conf. Proc. 291 (1980), pp. 10.1 to 10.34.

[3] *W. Schmidt, A. Jameson, D. Whitfield:* Finite volume solutions for the Euler equations for transonic flow over airfoils and wings including viscous effects. AIAA Paper 81-1265 (1981).

[4] *J. Longo, A. Jameson, W. Schmidt:* Dofoil – A viscous analysis program for transonic airfoil flow. Dornier FB 81 (1981).

[5] *A. Jameson:* Acceleration of transonic potential flow calculation on arbitrary meshes by the multiple grid method. AIAA Paper 79-1458 (1979).

[6] *S. Leicher:* Viscous flow simulation on high lift devices at subsonic and transonic speed. AGARD Conf. Proc. 291 (1980), pp. 6.1 to 6.15.

[7] *H. W. Stock:* Integralverfahren zur Berechnung dreidimensionaler, laminarer und turbulenter Grenzschichten. Dornier FB 77/51 B (1977).

[8] *R. Michel:* Etudes de la transition sur les profiles d'aile, établissement d'un critère de determination du point de transition et calcul de la trainée de profil en incompressible. ONERA Rap. 1/11578-A (1951).

[9] *S. H. Goradia* and *V. Lyman:* Laminar stall prediction and estimation of c_{Lmax}. J. Aircraft **11** (1974), pp. 528–536.

[10] *H. P. Horton:* Laminar separation bubbles in two- and three-dimensional incompressible flow. Ph. D. Thesis, Queen Mary College, University of London 1967.

[11] *H. P. Horton:* Entrainment in equilibrium and non-equilibrium turbulent boundary layers. Hawker Siddeley Aviation Ltd., Hatfield, Rep. Research / 1094 / HPH (1969).

[12] *H. B. Squire* and *B. A. Young:* The calculation of profile drag of airfoils. ARC R. & M. 1838 (1937).

[13] *X. Vaucheret:* Data Report on the CAST-7 profile in the ONERA S3MA Wind Tunnel. TR 201/1464 GN (1982).

[14] *R. C. Lock:* Report on a combined experimental and theoretical investigation of the airfoil CAST 7. RAE TR 79073 (1973).

[15] *F. Bauer, P. R. Garabedian, D. G. Korn, A. Jameson:* Supercritical wing sections II. Lecture Notes in Economics and Mathematical Systems No. 108. Springer-Verlag, Berlin/Heidelberg/New York 1976.

[16] *M. R. Collyer* and *R. C. Lock:* Improvements to the viscous Garabedian and Korn (VGK) method for calculating transonic flow past an airfoil. RAE TR 78039 (1978).

[17] *P. H. Cook, M. A. McDonald, M. C. F. Firmin:* Airfoil RAE 2822 pressure distribution and boundary layer measurements. Experimental data base for computer program assessment. AGARD-AR-138 (1979).

[18] *R. E. Melnik, R. Chow, H. R. Mead, A. Jameson:* An improved viscid/inviscid interaction procedure for transonic flow over airfoils. NASA CR (to be issued 1981).

[19] *Le Balleur:* Viscid-inviscid coupling calculations for two and three dimensional flows. Von Kármán Institute, Rhode-Saint-Genèse, Lecture Series 1982-04: Computational Fluid Dynamics (1982).